Tissue Specificity of Nonlinear Dynamics in Baseline fMRI

Gopikrishna Deshpande, Stephen LaConte, Scott Peltier, and Xiaoping Hu*

In this work, recent advances in the field of nonlinear dynamics (NLD) were applied to fMRI data to examine the spatio-temporal properties of BOLD resting state fluctuations. Five human subjects were imaged during resting state (visual fixation) at 3T using single-shot gradient echo planar imaging (EPI). Respiration and cardiac signals were concurrently recorded for retrospectively removing fluctuations due to these physiologic activities. Patterns of singularity in the complex plane (PSC) and Lempel-Ziv complexity (LZ) were used to study the deterministic nonlinearity in resting state fMRI data. The results show that there is greater nonlinearity (higher PSC) and determinism (lower LZ) in gray matter compared to white matter and CSF. In addition, the removal of respiratory and cardiac pulsations decreases the nonlinearity and determinism but does not alter the relative difference between gray matter and white matter. Therefore, our results demonstrate that determinism and nonlinearity in the fMRI data are tissue-specific, suggesting that they reflect native physiologic and metabolic fluctuations and are not a result of physiologic artifacts due to respiration and cardiac pulsation. Magn Reson Med 55:626–632, 2006. © 2006 Wiley-Liss, Inc.

Key words: baseline fMRI; tissue specificity; physiologic correction; nonlinear dynamics; functional connectivity

Functional magnetic resonance imaging (fMRI) is an important tool for understanding the workings of the brain in both the normal and diseased states. In BOLD fMRI, the brain is imaged over time with an MRI sequence sensitive to blood flow parameters to monitor localized hemodynamic response to neuronal metabolic activity. Since its inception, fMRI has become a routinely used approach for mapping brain function. Despite its widespread use, many mechanistic issues of the fMRI signal and its noise characteristics are not well understood and are still a topic of active research.

It has been reported (1) that fluctuations in fMRI data cannot be fully attributed to NMR noise and that the noise structure of the fMRI data may provide insights into the brain. In particular, fluctuations at very low frequencies (0.1 Hz) in fMRI data are spatially correlated within networks corresponding to related brain functions. This low frequency correlation has been utilized in the study of functional connectivity (2,3) and has been shown to reflect pathologic and/or physiologic alterations (4,5). The resting state (absence of explicit brain activation) is important because it conveys valuable information on basal neural activity. In addition, while we do not focus on a specific brain network here, these data have received increased attention with respect to diagnostic utility (4,5) and with proposed theories of the default mode of brain function (6).

The neuroscience community has learned a lot about the spatio-temporal nature of brain function through functional connectivity studies using various statistical approaches, including linear correlations between spatial regions (2,3,7), and data driven techniques such as principal component analysis (8) and self organizing maps (9). However, there is still great potential for building this knowledge base with alternative approaches. Linear statistical methods make an underlying assumption that the signals are produced by a linear stochastic system. Arguments based on brain physiology, however, suggest that the brain is likely to act as a nonlinear system that is not completely stochastic (10–14) and the processes generating fMRI data are expected to be nonlinear. Although existing linear methods work to a certain extent because a linear system can always approximate the behavior of a nonlinear system, nonlinear approaches may be more pertinent and sensitive, revealing additional insights into the fMRI data. Therefore, nonlinear methods for the analysis of fMRI data have been investigated in this work. Even though there has been an effort to study the nonlinearity of the BOLD response to explicit tasks (15–17), very little work has been done in applying methods of nonlinear dynamics to fMRI, particularly during the resting state. Building upon our preliminary study (18,19), we focus here on a systematic study of the tissue specific properties of nonlinear dynamics in fMRI resting state data.

In addition to possibly revealing interesting patterns in the resting state brain dynamics, nonlinear analysis may allow us to better characterize biologic sources of noise in the MRI signal. Kruger et al. reported higher random fluctuations in the gray matter (1); this may be due to deterministic nonlinearity of the signal produced by an underlying finite dimensional system. If the driving sources of these fluctuations are of nonlinear origin, they should also be revealed with nonlinear analysis techniques. Further, an enhanced ability to characterize the biologic noise may allow us to reduce its effect on activation detection.

As described in the following sections, the present work examines several aspects of nonlinear dynamics. We start by reconstructing the state space of the system and finding a finite minimum embedding dimension (MED) of the underlying system. The nonlinearity arising from the finite dimensional dynamics are then characterized using patterns of singularities in the complex plane (PSC). How-

Department of Biomedical Engineering, Georgia Tech/Emory, Atlanta, GA, USA.

Grant Sponsor: Georgia Research Alliance. Grant Sponsor: NIH; Grant Number: EB002009.

*Correspondence to: Xiaoping Hu, Ph.D., Wallace H. Coulter Department of Biomedical Engineering, Georgia Institute of Technology and Emory University, 101 Woodruff Circle, Suite 2001, Atlanta, GA 30322, USA. E-mail: xhu@bme.emory.edu

Received 6 July 2005; revised 5 November 2005; accepted 22 November 2005.

DOI 10.1002/mrm.20817

Published online 7 February 2006 in Wiley InterScience (www.interscience.wiley.com).

ever, the nonlinearity may arise either due to stochastic or deterministic dynamics. We thus evaluate the determinism in the dynamics to make this distinction. A finite embedding dimension is a measure of the determinism of the system, which can be quantified using information theoretic measures like Lempel-Ziv complexity. It is widely recognized by many that physiologic noise due to respiration and cardiac pulsation can be a significant contribution to the signal fluctuation in fMRI (1,20). Therefore, it is also of interest to study their contribution to the nonlinear dynamics in the fMRI signal. A minor aspect of the present work looks at this effect by applying the nonlinear analysis to data before and after physiologic noise correction. Our approach, then, is to obtain a comprehensive understanding of resting state fMRI by estimating the appropriate embedding dimension and subsequently characterizing the system dynamics using nonlinearity and determinism.

THEORY

Linear methods can capture structures in a signal like dominant frequency and linear correlations. This relies on the assumption that the intrinsic dynamics are governed by the linear paradigm that small causes lead to small effects. Since the possible solutions of linear equations are either exponential or periodic oscillation, the irregular structure in the signal has to be attributed to some random external input to the system producing the signal. However, recent advances in chaos theory have brought to light the fact that a random input is not the only possible source of irregularity in a system's output. Nonlinear chaotic systems can produce very irregular data with purely deterministic governing equations. One way to evaluate whether a system is deterministic or random is to estimate the minimum embedding dimension (MED) (21–27), which is the number of independent state variables contributing to the irregular dynamics of a signal (e.g., an fMRI time series). (Please refer to the Appendix for details about calculation of MED.) Once the finite dimensionality of a system has been established through MED, it is possible to characterize the nonlinearity and determinism using methods described below.

Pattern of Singularities in the Complex Plane (PSC) Algorithm

It has been found that the distribution of singularities in the complex plane is critical for determining the behavior of a dynamical system at any arbitrary time. From numerical investigations of the Lorenz equations (28), it was demonstrated that when the system is in a periodic regime (limit cycle) the arrangement of singularities (poles) reflects the corresponding periodicity of the real-time solution. As the dynamical regime transitions toward the chaotic one, the corresponding arrangement of singularities becomes very irregular. From these results, Di Garbo (29) suggested an algorithm (the PSC algorithm) to evaluate the nonlinear structure in a time series. The method determines a measure of significance, using a null hypothesis that the time series under investigation arises from a linear process. The null hypothesis is rejected if the value of this significance is greater than a threshold (say, 95% confidence level). The significance value can be further used as a quantifier to assess deviation from linearity. The larger its value, the more nonlinear is the time series. (Please refer to the Appendix for details of the PSC algorithm.)

Since the PSC algorithm looks for only the nonlinear signal structure, it cannot be concluded from this measure alone whether the nonlinearity is due to deterministic dynamics or stochastic dynamics. To answer this question, the Lempel-Ziv complexity measure is considered.

Lempel-Ziv Complexity Measure Algorithm

The Lempel-Ziv complexity measure (LZ) is a unique way of looking at the structure of the signal (30). The signal must first be transformed into a finite symbol sequence S. If we have a string $s_1,s_2,\ldots,s_n$, then $c(n)$, which is the number of different sub-strings of $s_1,s_2,\ldots,s_n$, is the measure of complexity. It reflects the rate of new patterns arising with increasing sequence length, n. Thus, by simple operations of comparison and accumulation, the computation of $c(n)$ is achieved. In this article, we have used the normalized complexity measure $C(n)$, which is the ratio of $c(n)$ to $b(n)$, where $b(n)$ gives the asymptotic behavior of $c(n)$ for a random string. LZ is zero for a fully deterministic signal and one for a totally random signal. Hence, LZ indicates the degree of determinism in the signal. (Please refer to the Appendix for details of the LZ algorithm.)

METHODS

MRI Data Acquisition and Analysis

Data acquisition consisted of imaging 3 normal, healthy human subjects in resting state using a single-shot BOLD-contrast gradient EPI sequence at 3T Siemens Trio (TR = 750 ms, TE = 34 ms, Flip Angle = 50 deg, and FOV = 22 cm, with 5 contiguous axial slices covering the region from the top of the head to the top of the corpus collosum, 5 mm slice thickness, 1120 volumes (time points) per slice, and 64 phase and frequency encoding steps). Two additional volunteers were scanned using the same parameters as above, but with 10 saggital (rather than axial) slices containing the ventricles. High resolution (512 $\times$ 512) T_1-weighted axial anatomic images were acquired in the first scanning session. In the second session, anatomic images with 1 mm isotropic resolution were acquired using a magnetization prepared rapid gradient echo (MPRAGE) sequence (31) (TR/TE/FA of 2600 ms/3.93 ms/8 deg).

For the anatomic data from the first session, the images were segmented using a procedure involving manual removal of the extra-cranial signal and segmentation of gray and white matter based on their intensity. The resulting segmented images were down-sampled by a factor of 8 to obtain a 64 $\times$ 64 mask of gray matter and white matter. The MPRAGE images in the second experiment were segmented into gray matter, white matter, and CSF using SPM2 (Wellcome Department of Cognitive Neurology, London, UK; http://www.fil.ion.ucl.ac.uk). Since SPM2 segments the images in the normalized space, the resulting masks were transformed back into the original image

Table 1
Typical Values of the PSC Nonlinearity Index for Simulated and Commonly Occurring Physiological Signals

Type of signal	Typical PSC nonlinearity score	
	Without noise	With noise
Linear stochastic process	2	5
Deterministic function	6	8
Respiration	26–60	30–70
EKG	10–30	17–35
EEG		
Background	175	182
Alpha activity	1500	1549
Baseline fMRI	400–2000	420–2017

space, resliced to match the location of the EPI data, and thresholded to obtain binary masks of the 3 tissue types. The resulting masks were similarly down-sampled to the resolution of the EPI images.

A physiologic monitoring unit consisting of a pulse-oximeter and nasal respiratory canula was used during data acquisition to record cardiac and respiratory pulsations, respectively. These physiologic fluctuations were corrected for in the functional data retrospectively (20). Both physiologically corrected and uncorrected data were analyzed and compared.

Nonlinear Dynamical Analysis

The strategy employed for the application of the NLD methods is outlined below. A MATLAB program was developed and utilized for all the analysis described below. The MED of baseline fMRI was first calculated using the modified false nearest neighbor approach (27). A low finite value of MED was obtained, which provided a justification for the characterization of nonlinearity using PSC. A high value of nonlinearity in resting-state fMRI prompted us to investigate the source of this nonlinearity (deterministic or stochastic) by employing the information-theoretic measure, LZ. The PSC and LZ values were calculated for each voxel in all the axial slices for subjects 1, 2, and 3 and all saggital slices for subjects 4 and 5. The mean values of the nonlinear measures for each tissue type were obtained and tabulated. Since the resultant parameters for each tissue type were not normally distributed, the statistical significance of the tissue difference of each measure was assessed using the nonparametric Wilcoxon rank sum test (32). Also, PSC and LZ values were used to generate summary images for visualization. These strategies enabled us to characterize baseline fMRI dynamics using deterministic nonlinearity.

RESULTS AND DISCUSSION

The MED values were calculated by reconstructing the attractor for each voxel time series in all the slices as outlined in the previous section. The mean MED for gray matter, white matter, and CSF was found to be 10.55 ± 0.97, 10.89 ± 0.96, and 9.6 ± 1.12, respectively, which indicated that the difference in means was not significant and, hence, the embedding dimension was not tissue-specific. Since MED is an integer number, we rounded off the value to 10. The MED results suggest that a finite number of state variables describe the baseline fMRI dynamics and thus provide a justification for the quantification of nonlinearity using the PSC measure. We have calculated the PSC measure from simulated signals and various biologic time series—cardiac and respiratory data obtained from the physiologic monitoring unit during our fMRI data acquisition, EEG signal obtained from MIT-BIH data base (http://circ.ahajournals.org/cgi/content/full/101/23/e215), and the fMRI data from the present study. Normally distributed random numbers were generated to emulate signals of a linear stochastic process, and a sinusoidal signal was used as an example of a deterministic signal. Both types of signal had the same number of time points as the experimental time series (1120 points). Table 1 lists the PSC for the various types of signals described above with and without the addition of 10 dB Gaussian noise. The high value of PSC for fMRI data confirms the nonlinear structure in the signal. The results also indicate that PSC is fairly robust to random noise.

Figure 1 shows the PSC map of an axial slice of the human cortex for subject 3. It may be observed from the figure that there is more nonlinearity in gray matter than white matter. This conclusion is quantitatively validated by the mean PSC values given for white matter, gray matter, and CSF in Table 2. Statistically, there is a highly significant difference in the PSC values between the 3 tissue types, with gray matter showing significantly higher nonlinearity than white matter and CSF. As previously mentioned, the study by Kruger et al. (1) has shown that gray matter exhibits more random fluctuations compared to white matter. Our PSC results indicate nonlinear signal structure, but do not reveal whether the nonlinearity arises from deterministic dynamics or stochastic dynamics. The LZ results can be used to answer this question. Figure 2 shows the LZ map for an axial slice from subject 3. Table 3 shows the mean values of LZ for all 3 tissues types. Since the values of LZ are less than one, there is evidence of determinism. Lower values for gray matter indicate higher determinism compared to white matter and CSF. Even though there is heterogeneity of PSC and LZ within a

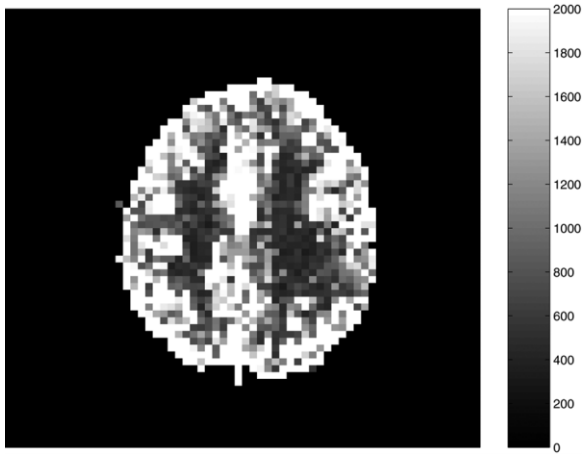

FIG. 1. PSC map for an axial slice from subject 3.

Table 2
PSC Values for Gray Matter, White Matter, and CSF

PSC	Gray matter	White matter	CSF	Wilcoxon sum rank test: *P*-value		
				GM-WM	GM-CSF	WM-CSF
Subject 1	765	457	-	8.68×10^{-12}	-	-
Subject 2	1065	634	-	2.39×10^{-12}	-	-
Subject 3	1080	645	-	0	-	-
Subject 4	962	716	841	6.9×10^{-5}	1.5×10^{-5}	4.8×10^{-4}
Subject 5	940	771	618	3.1×10^{-5}	3.2×10^{-4}	3.1×10^{-5}

tissue type, the *P*-values from the Wilcoxon sum rank test showed that their distributions are significantly different for the 3 tissues.

The inter-subject variability in the values can be attributed to the fact that the "resting state" or "baseline" is not a well-defined state and can be highly variable from subject to subject. Also, we can see from Tables 2 and 3 that gray matter exhibits higher nonlinear determinism than white matter at a statistically significant level. This tissue specificity can be attributed both to the differences in fMRI physiology and neural processing. The BOLD contrast in fMRI is a result of interactions between cerebral blood flow (CBF) and cerebral blood oxygenation (CBO). It has been shown that CBF fluctuations result in CBO fluctuations (33). There are several arguments for and against blood pressure (34) and vasomotion (35) as being the source of fluctuations in CBF. Native fluctuations in CBF arising from fluctuations in NADH and HBO_2 can be attributed to such fluctuations in cortical metabolism and neuronal activity (36). These give rise to a complex interplay of various factors that result in baseline fMRI signal fluctuations. The regional differences in the interplay between these factors likely give rise to the differences in fMRI signal fluctuations from different tissues structures. These signal differences have been characterized numerically in this article using nonlinear analysis. This complements previous studies that have indicated that there is non-uniform determinism across activities (37) in the brain. Interestingly, our results seem to indicate that there is non-uniform determinism across different regions of the brain as well.

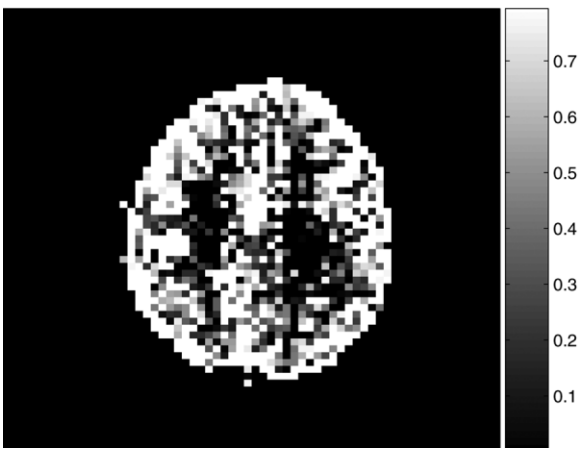

FIG. 2. 1-LZ map for an axial slice from subject 3.

An important fact to consider is the effect of removal of physiologic noise on the results. To investigate the spatial extent of the effect of correction, we plotted the difference images (original - corrected) of the PSC and LZ parameters. Figures 3a and 3b show the PSC and LZ difference images, respectively, for an axial slice. For comparison, Fig. 3c illustrates the percentage reduction in signal variance after correction in the same axial slice. It can be seen that a greater amount of noise is removed in gray matter and CSF than in white matter, indicating higher physiologic noise in them. This observation is consistent with higher noise in gray matter compared to white matter, reported by Kruger et al. (1), attributed to possible differences in blood volume and perfusion in those tissues. By carrying out the analysis on physiologic noise-corrected data, we have accounted for the differences in fMRI noise characteristics arising from cardiac and respiratory pulsations. The similarity between Figs. 3a, 3b, and 3c indicates that the nonlinearity and determinism contributed by the physiologic rhythms is mostly removed by retrospective correction.

To test if the difference in noise level between gray matter and white matter as reported by Kruger (1) is a major cause of the observed gray-white difference in nonlinear determinism, Gaussian random noise was added to white matter time courses to match their SD to that of gray matter time series, and PSC and LZ were calculated on these synthetic white matter time courses. From the results shown in Table 4, the PSC for the synthetic white matter time courses, although slightly increased, is still much less than that of gray matter shown in Table 2. This is consistent with the notion that Gaussian noise is a linear process and is not expected to increase the nonlinearity significantly. In Table 4, the noise addition slightly increases the LZ, as expected since the addition of random noise decreases determinism (and, hence, increases LZ), moving the LZ of synthetic white matter time courses further away from that of gray matter. Given these observations, it is unlikely that the increased noise level in gray matter is a major cause for the tissue specificity of deterministic nonlinearity.

To ascertain the nonlinear determinism of the CSF, we carried out a similar analysis on saggital slices, including an ROI on ventricles. Figures 4a, 4b, and 4c illustrate the PSC and LZ difference images and percentage reduction in fMRI signal variance due to correction, respectively, for a representative saggital slice containing the ventricles. It is well known that CSF has higher physiologic noise compared to gray matter and white matter. This notion is confirmed in Fig. 4c, which shows greater noise reduction in the ventricles compared to the cortical gray/white mat-

Table 3
LZ Values for Gray Matter, White Matter, and CSF

LZ	Gray matter	White matter	CSF	Wilcoxon sum rank test: *P*-value		
				GM-WM	GM-CSF	WM-CSF
Subject 1	0.82	0.91	-	2.28×10^{-12}	-	-
Subject 2	0.60	0.72	-	3.05×10^{-7}	-	-
Subject 3	0.64	0.82	-	3.89×10^{-25}	-	-
Subject 4	0.56	0.69	0.75	2.5×10^{-6}	8.9×10^{-4}	8.5×10^{-7}
Subject 5	0.65	0.70	0.73	3.7×10^{-4}	2.2×10^{-3}	5.3×10^{-5}

ter, leading to greater differences in PSC and LZ values of CSF before and after correction. In particular, we found that the raw CSF pulsation, which contains the B-waves (38), is highly nonlinear. Retrospective correction substantially decreased the variance in CSF time courses as well its nonlinearity and determinism. In contrast, the decrease in nonlinearity and determinism in gray and white matter after correction was insignificant compared to that of CSF. It is worth noting that physiologic correction only scaled down the nonlinearity and determinism, preserving its tissue specificity. Therefore, the tissue specificity of deterministic nonlinearity we report is unlikely to arise solely from cardiac and respiration effects. Rather, fMRI physiology and the nature of neural processing (reflected by the native fluctuations) vary across tissues, giving rise to the tissue-specific nature of the baseline signal.

CONCLUSIONS

This study approaches the processing of fMRI data from a nonlinear dynamical perspective. We have shown that fMRI time courses are not produced by a purely stochastic system and, hence, have used various nonlinear techniques to obtain a new perspective into the underlying system dynamics. The results from the above techniques show that brain dynamics can be characterized neither by a purely stochastic nor a fully deterministic system. On the contrary, the underlying dynamics seems to be deterministic, produced by a system having roughly 10 state variables, exhibiting non-uniform determinism among the different regions of the brain, with gray matter showing more determinism than white matter and CSF. What was previously perceived as higher random fluctuation in the gray matter is actually due to the deterministic nonlinearity of the signal produced by an underlying nonlinear dynamical system. We found that the nonlinearity exhibits tissue specificity even after the removal of physiologic fluctuations. The possibility of higher noise level in gray matter as a main reason for tissue-specificity of deterministic nonlinearity was examined and ruled out. Therefore, higher nonlinear determinism in gray matter is not due to cardiac/respiratory effects or noise intensity differences, but can potentially be attributed to local differences in fMRI physiology and neural processing.

APPENDIX

Estimation of MED

The technique we have employed is a variant of the False Nearest Neighbor (FNN) method and follows the description by Cao et al. (27). The first step in nonlinear dynamical analysis is the reconstruction of the attractor in phase-space using Taken's embedding theorem (39), which ensures that the reconstructed attractor preserves all topological properties of the original attractor.

Given a voxel fMRI time series, $x(i), i = 1,2, \ldots, L$, its time-delay vectors in phase-space are formed as:

$$X = [X_1, X_2, \ldots, X_N]^T \quad [1]$$

where the number of time-delay vectors is given by $N = L - (m-1)\tau$, with τ being the time delay and m being the embedding dimension. Each time-delay vector is given by

$$X_i = [x(i+\tau), x(i+2\tau), \ldots, x(i+(m-1)\tau]; \quad i = 1,2, \ldots, L-(m-1)\tau \quad [2]$$

τ is selected using the autocorrelation function based technique (26).

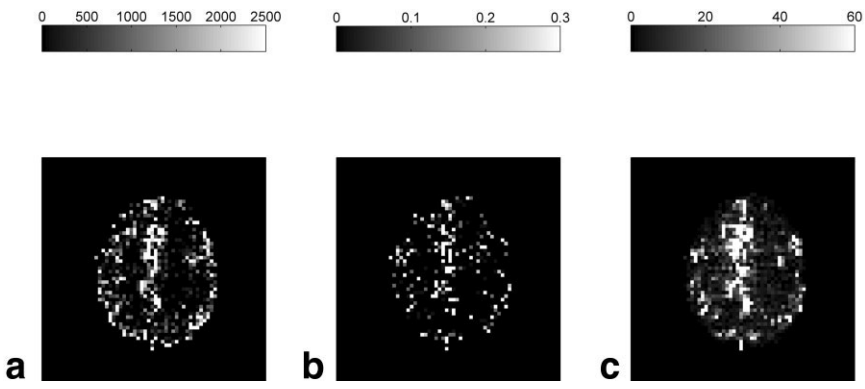

FIG. 3. (**a**) PSC difference map (original value- corrected value) for an axial slice. (**b**) LZ difference map for the same slice. (**c**) Percentage reduction in fMRI time course variance after physiologic correction for the same slice.

Table 4
White Matter PSC and LZ Obtained Before and After the Addition of White Gaussian Noise to Match the Noise Variance of Gray Matter Time Courses

Sub	Before noise addition		After noise addition	
	PSC	LZ	PSC	LZ
1	457	0.91	481	0.98
2	634	0.72	684	0.90
3	645	0.82	676	0.98
4	716	0.69	737	0.82
5	771	0.70	789	0.84

For each phase-space vector, $\boldsymbol{X}_i$, its distance to its nearest neighbor at different values of m, $d(i, m)$, is computed. The ratio, $d(i, m + 1)/d(i, m)$, is calculated and averaged over i to derive $E(m)$. $E(m)$ is dependent only on m and τ. In order to see its variation from m to $m + 1$, we examine $E_1(m)$, defined as the ratio of $E(m + 1)$ to $E(m)$. It is found that $E_1(m)$ approaches a saturation value of 1 when m is greater than some value m_0 if the time series comes from an attractor.

To determine the m_o at which E_1 attains saturation, a nonlinear least-squares fit to E_1 is obtained (40). The fit is assumed to be of an exponential form given by the equation $b - e^{-m-c}$, where the initial values of b and c are 1 and 0, respectively. The values of b and c corresponding to the closest fit are obtained using the Gauss-Newton method (40). The residual, which is the error between the fit and the original curve, is the highest at the knee of the curve. Since the saturation point is represented by the knee of the curve, the dimension corresponding to the maximum residual is taken as the MED.

Pattern of Singularities in the Complex Plane (PSC) Algorithm

The steps for deriving PSC of a given fMRI time series are:

1. Determine the local maximum s_{t_j} and the time at which it occurred, t_j, in the fMRI time series, where j is the index for each maximum and assumed to have values $1,2,\ldots\ldots m$.
2. Define L_o as a global distance measure in the s_t-t space:

$$L_0 = \sqrt{\sum_{j=1}^{m-1}\{(s_{t_{j+1}} - s_{t_j})^2 + (t_{j+1} - t_j)^2\}} \quad [4]$$

3. Generate n number of surrogates and compute L_o for each surrogate. Gaussian scaled surrogates were generated by rank ordering the fMRI time series in the rank order of the time series obtained from a phase-randomized Gaussian distribution of the same mean and SD as that of the fMRI data (29).
4. Determine mean M_L and SD σ_L of these quantities.
5. Determine the measure of significance.

$$S_{psc} = \frac{|L_o - M_L|}{\sigma_L} \quad [5]$$

The hypothesis (that the given time series is not different from a linear process) is rejected if this significance is greater than a threshold (for this work, we have chosen the 95% confidence level). Moreover, the significance value is the PSC measure, which can be used as a quantifier to assess the deviation of the fMRI time series from linearity. The larger its value, the more nonlinear is the fMRI time series.

The Lempel-Ziv Complexity Measure Algorithm

The Lempel-Ziv Complexity Measure (LZ) is a complexity measure for assessing the structure of a signal (30) from an information theoretic point of view. The algorithm for calculating this complexity measure $c(n)$ for a given fMRI time series $x(i)$ of length n can be summarized as follows: $x(i)$ must be first transformed into a finite symbol sequence L with two possible binary values: zero and one. We start by subtracting the mean value of $x(i)$ from every data point. We need to find a threshold T to transform $x(i)$ into a binary sequence. The threshold is found as follows: The positive peak value U_p and negative peak value U_n of $x(i)$ are calculated. The number of data points of $x(i)$ that satisfy the condition $0 < x_i < 10\% U_p$ is calculated. Let this number be A. Similarly, the number of data points of $x(i)$

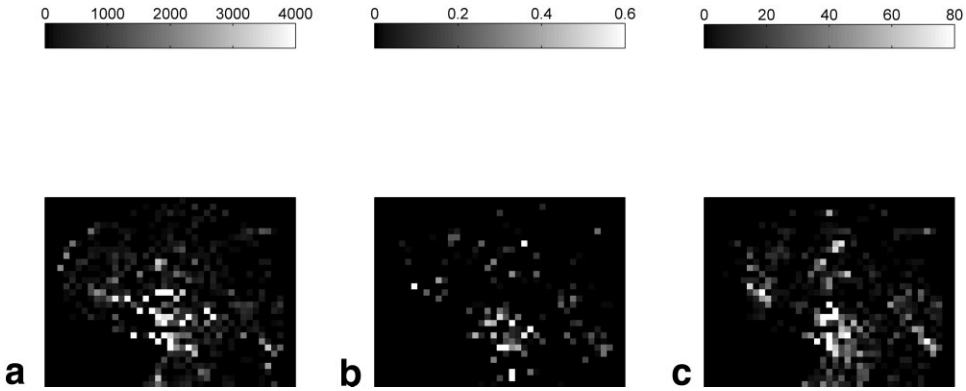

FIG. 4. (**a**) PSC difference map (original value- corrected value) for a saggital slice. (**b**) LZ difference map for the same slice. (**c**) Percentage reduction in fMRI time course variance after physiologic correction for the same slice.

satisfying the condition $10\%U_n < x_i < 0$ is calculated. Let this number be B. If $(A + B) < 40\%$ of n, threshold $T = 0$. If $(A < B)$, $T = 20\%\ U_p$ *else*, $T = 20\%\ U_n$. The value of each data point of the fMRI time series $x(i)$ is compared with T and assigned a value of 0 or 1 depending on whether its value is below or above T. The finite binary sequence L is used for further analysis.

Let us consider the sequence $L = s_1,s_2,\ldots,s_n$, where s_i is the character 0 or 1. Let M and N be two sub-strings of L and let MN be their concatenation. We will denote MN' as the sequence MN without its last character. Initially, $c(n)$ is set to 1. Therefore, $c(n) = 1$, $M = s_1$, $N = s_2$, $MN = s_1s_2$, and $MN' = s_1$. If $M = s_1,s_2,\ldots,s_r$ $(1 < r < n)$ and $N = s_{r+1}$, then $MN' = s_1,s_2,\ldots,s_r$. The value of $c(n)$ is incremented by one if $N \notin MN'$. If $N \in MN'$, then N is a sub-sequence of MN' and not a new sequence. Therefore, M remains unchanged and N is renewed to s_{r+1}, s_{r+2}. The process of appending and comparing N to MN' is continued until $N \notin MN'$ again. As the whole sequence L is traversed, the value of $c(n)$ is also updated. The final value of $c(n)$ obtained by traversing the whole length of L is the complexity measure. Normalization of the final $c(n)$ results in the LZ measure. Let $d(n)$ be the value of $c(n)$ in the asymptotic case of an infinitely long random string. Then,

$$d(n) = \lim_{n\to\infty} c(n) = \frac{n}{\log_2 n} \qquad [6]$$

Finally, the normalized complexity measure, LZ, is given by

$$c(n)/d(n) \qquad [7]$$

REFERENCES

1. Kruger G, Glover GH. Physiological noise in oxygenation-sensitive magnetic resonance imaging. Magn Reson Med 2001;46:631–637.
2. Biswal B, Yetkin FZ, Haughton VM, Hyde JS. Functional connectivity in the motor cortex of resting human brain using echo-planar MRI. Magn Reson Med 1995;34:537–541.
3. Lowe MJ, Mock BJ, Sorenson JA. Functional connectivity in single and multislice echoplanar imaging using resting-state fluctuations. NeuroImage 1998;7:119–132.
4. Quigley M, Cordes D, Wendt G, Turski P, Moritz C, Haughton V, Meyerand ME. Effect of focal and nonfocal cerebral lesions on functional connectivity studied with MR imaging. Am J Neuroradiol 2001; 22:294–300.
5. Li SJ, Li Z, Wu GH, Zhang MJ, Franczak M, Antuono PG. Alzheimer disease: Evaluation of a functional MR imaging index as a marker. Radiology 2002;225:253–259.
6. Raichle ME, MacLeod AM, Snyder AZ, Powers WJ, Gusnard DA, Shulman GL. A default mode of brain function. Proc Natl Acad Sci USA 2001;98:676–682.
7. Peltier SJ, Noll DC. T2* dependency of low frequency functional connectivity. Neuroimage 2002;16:985–992.
8. Strother SC, Anderson JR, Schaper KA, Sidtis JJ, Liow JS, Woods RP, Rottenberg DA. Principal component analysis and the scaled sub-profile model compared to inter-subject averaging and statistical parametric mapping. I. "Functional connectivity" of the human motor cortex studied with [^{15}O] water PET. J Cereb Blood Flow Metab 1995;15:738–753.
9. Peltier SJ, Polk TA, Noll DC. Detecting low-frequency functional connectivity in fMRI using a self-organizing map (SOM) algorithm. Hum Brain Mapp 2003;20:220–226.
10. Elbert T, Ray WJ, Kowalik ZJ, Skinner JE, Graf KE, Birbaumer N. Chaos and physiology: deterministic chaos in excitable cell assemblies. Physiol Rev 1994;74:1–47.
11. Schiff SJ, Jerger K, Duong DH, Chang T, Spano ML, Ditto WL. Controlling chaos in the brain. Nature 1994;370:615–20.
12. Wagner CD, Persson PB. Nonlinear chaotic dynamics of arterial blood pressure and blood flow. Am J Physiol 1995;268:H621–627.
13. Babloyantz A, Destexhe A. Low dimensional chaos in an instance of epilepsy. Proc Natl Acad Sci USA 1986;83:3513–3517.
14. Freeman WJ. Role of chaotic dynamics in neural plasticity. Prog Brain Res 1994;102:319–333.
15. Vazquez AL, Noll DC. Nonlinear aspects of the BOLD response in Functional MRI. Neuroimage 1998;7:108–118.
16. Friston KJ, Josephs O, Rees G, Turner R. Nonlinear event-related responses in fMRI. Magn Reson Med 1998;39:41–52.
17. Birn RM, Saad ZS, Bandettini PA. Spatial heterogeneity of the nonlinear dynamics in the FMRI BOLD response. Neuroimage 2001;14:817–826.
18. LaConte S, Ngan S, Zhuang J, Heberlein K, Peltier S, Hu X. Evidence for nonlinear dynamical determinism related to functional connectivity in fMRI baseline time series. In: Proceedings of the 11th Annual Meeting of ISMRM, Toronto, Canada, 2003. p. 1178.
19. LaConte S, Peltier S, Kadah Y, Ngan S, Deshpande G, Hu X. Detecting nonlinear dynamics of functional connectivity. Proc SPIE Intl Soc Opt Eng 2004;5369:227–237.
20. Hu X, Le TH, Parrish T, Erhard P. Retrospective estimation and correction of physiological fluctuation in functional MRI. Magn Reson Med 1995;34:201–212.
21. Grassberger P, Procaccia I. Characterization of strange attractors. Phys Rev Letters 1983;50:346–349.
22. Broomhead DS, King GP. Extracting qualitative dynamics from experimental data. Physica D 1986;20:217–236.
23. Mees AI, Rapp PE, Jennings LS. Singular value decomposition and embedding dimension. Phys Rev A 1987;37:340–346.
24. Theiler J. Efficient algorithm for estimating the correlation dimension from a set of discrete points. Phys Rev A 1987;36:4456–4462.
25. Kennel MB, Brown R, Abarbanel HDI. Determining minimum embedding dimension using a geometrical construction. Phys Rev A 1992;45: 3403–3411.
26. Tsonis AA. Chaos—from theory to applications. 1992. New York: Plenum Press.
27. Cao L. Practical method for determining the minimum embedding dimension of a scalar time series. Physica D 1997;110:43–50.
28. Tabor M, Weiss J. Analytic structure of the Lorenz system. Phys Rev A 1981;24:2157–2167.
29. Di Garbo A, Balocchi R, Chillemi S. Nonlinearity tests using the extrema of a time series. International J Bifurcation and Chaos 1998;8: 1831–1838.
30. Zhang XS, Zhu YS, Thakor NV, Wang ZZ. Detecting ventricular tachycardia and fibrillation by complexity measure. IEEE Trans Biomed Eng 1999;46:548–555.
31. Mugler J, Brookeman J. Three-dimensional magnetization-prepared rapid gradient-echo imaging (3D MP RAGE). Magn Reson Med 1990; 15:152–157.
32. Wilcoxon F. Individual comparisons by ranking methods. Biometrics 1945;1:80–83.
33. Obrig H, Neufang M, Wenzel R, Kohl M, Steinbrink J, Einhaupl K, Villringer A. Spontaneous low frequency oscillations of cerebral hemodynamics and metabolism in human adults. Neuroimage 2000;12:623–639.
34. Giller CA, Hatab MR, Giller AM. Oscillations in cerebral blood flow detected with a transcranial Doppler index. J Cereb Blood Flow Metab 1999;19:452–459.
35. Hudetz AG, Biswal BB, Shen H, Lauer KK, Kampine JP. Spontaneous fluctuations in cerebral oxygen supply. Adv Exp Med Biol 1998;454: 551–559.
36. Elwell CE, Springett R, Hillman E, Delpy DT. Oscillations in cerebral hemodynamics: implications for functional activation studies. Adv Exp Med Biol 1999;471:57–65.
37. Dhamala M, Pagnoni G, Wiesenfeld K, Berns GS. Measurements of brain activity complexity for varying mental loads. Phy Rev E 2002;65: 419171–419177.
38. Auer LM, Sayama I. Intracranial pressure oscillations (B-waves) caused by oscillations in cerebrovascular volume. Acta Neurochir (Wien). 1983;68:93–100.
39. Takens F. Detecting strange attractors in turbulence. 1980. In: Rand D, Young L, eds. Dynamical systems and turbulence, vol. 898. Berlin: Springer-Verlag. p 366–381.
40. Por LT, Puthusserypady S. Postprocessing methods for finding the embedding dimension of chaotic time series. Phy Rev E 2005;72: 027204.